The International Journal of Cardiovascular Imaging (2023) 39:2051–2061
https://doi.org/10.1007/s10554-023-02903-0

ORIGINAL PAPER

Multimodality coronary imaging to predict non-culprit territory unrecognized myocardial infarction in Non-ST-Elevation acute coronary syndrome

Masahiro Hoshino[1] · Tomoyo Sugiyama[1] · Yoshihisa Kanaji[1] · Masahiro Hada[1] · Tatsuhiro Nagamine[1] · Kai Nogami[1] · Hiroki Ueno[1] · Kodai Sayama[1] · Kazuki Matsuda[1] · Taishi Yonetsu[2] · Tetsuo Sasano[3] · Tsunekazu Kakuta[1]

Received: 13 February 2023 / Accepted: 16 June 2023 / Published online: 24 July 2023

Abstract

Purpose: Unrecognized myocardial infarction (UMI) detected by cardiac magnetic resonance (CMR) imaging is associated with adverse outcomes in patients with acute and chronic coronary syndrome. This study aimed to assess the predictors of optical coherence tomography (OCT) and coronary computed tomography angiography (CCTA) findings for non-infarct-related (non-IR) territory UMI in patients presenting with non-ST-elevation acute coronary syndrome (NSTE-ACS). Methods: We investigated 69 patients with a first clinical episode of NSTE-ACS who underwent pre-percutaneous coronary intervention (PCI) 320-slice CCTA, uncomplicated urgent PCI with OCT assessment within 24 h of admission, and post-PCI CMR. UMI was assessed using late gadolinium enhancement to identify regions of hyperenhancement with an ischemic distribution pattern in non-IR territories. Results: Non-IR UMI was detected in 11 patients (15.9%). Lower ejection fraction, higher Gensini score, higher Agatston score, high pericoronary adipose tissue attenuation (PCATA), OCT-defined culprit lesion plaque rupture, and OCT-defined culprit lesion cholesterol crystal were significantly associated with the presence of non-IR UMI. On dividing the total cohort was divided into five groups according to the numbers of two OCT-derived risk factors and two CCTA-derived risk factors, the frequency of non-IR UMI frequency significantly increased according to the number of these relevant risk features ($p < 0.001$). Patients with all of the non-IR UMI risk factors showed 50% prevalence of non-IR UMI, compared with 2.2% of patients with low risk factors (≤ 2). Conclusions: Integrated CCTA and culprit lesion OCT assessment may help identify the presence of non-IR UMI, potentially providing prognostic information in patients with first NSTE-ACS episode.

Keywords Acute coronary syndrome · Optical coherence tomography · Coronary computed tomography angiographic · Cardiac magnetic resonance · Unrecognized myocardial infarction

Introduction

A non-negligible proportion of myocardial infarctions (MI) occur in the absence of clinical manifestations. Unrecognized myocardial infarction (UMI) is increasingly recognized as an important contributor to the rising risk of adverse cardiac events in patients with both acute coronary syndrome (ACS) and chronic coronary syndrome (CCS) [1–3]. Late gadolinium enhancement (LGE) using cardiac magnetic resonance (CMR) imaging can detect even a small myocardial scar which is associated with a worse prognosis [4, 5].

Although the mechanisms causing UMI remain undetermined, pathological studies suggest that subclinical

✉ Tsunekazu Kakuta
kaz@joy.email.ne.jp

Masahiro Hoshino
masaedamasa@yahoo.co.jp

[1] Division of Cardiovascular Medicine, Tsuchiura Kyodo General Hospital, Ibaraki, Japan

[2] Department of Interventional Cardiology, Tokyo Medical and Dental University, Tokyo, Japan

[3] Department of Cardiovascular Medicine, Tokyo Medical and Dental University, Tokyo, Japan

episodes of plaque rupture could be associated with healed MI [6]. Culprit plaque vulnerability in patients was associated with pancoronary vulnerability and advanced atherosclerosis [7]. Previous reports showed that the vulnerability of non-culprit plaque was consistent with the culprit plaque vulnerability in patients with ACS [8, 9]. However, the association between the presence of non-infarct-related territory (non-IR) UMI and in vivo coronary plaque characteristics of the culprit vessel in patients with ACS remains elusive.

Recent reports support the clinical potential of predicting the existence of non-IR UMI using coronary computed tomography angiography (CCTA) in patients with non-ST-segment elevation acute coronary syndrome (NSTE-ACS) [10, 11], whereas predictors of non-IR UMI using optical coherence tomography (OCT) findings of culprit lesions remain unknown. Furthermore, the association between the presence of UMI and multimodality coronary imaging findings, including CCTA and OCT, remains unknown. Therefore, the aim of the present study was to assess the predictors of OCT and CCTA findings for non-IR UMI evaluated by delayed enhancement-CMR (DE-CMR) in patients presenting with a first episode of NSTE-ACS without a history of MI.

Methods

Study design and patient population

This study was a retrospective subgroup analysis of prospectively, but non-consecutively, enrolled patients in the institutional NSTE-ACS CCTA research registry at Tsuchiura Kyodo General Hospital, as previously described [12, 13]. From this registry, we included 69 patients with a first clinical episode of NSTE-ACS between January 2013 and May 2020, who underwent pre- percutaneous coronary intervention (PCI) 320-slice CCTA, uncomplicated urgent PCI with OCT assessment within 24 h of admission, and post-PCI CMR at the median of 8 days (5–12) from PCI. We included patients with NSTEMI and unstable angina pectoris when a single culprit lesion was identifiable and was considered suitable for PCI. NSTEMI was defined as ischemic symptoms in the absence of ST-segment elevation on electrocardiography with elevated cardiac biomarker levels (14). Unstable angina pectoris was defined as newly developed or accelerating chest symptoms on exertion or rest angina within 2 weeks without biomarker release.

In cases of multivessel disease, DE-CMR imaging was performed before staged non-IR lesion revascularization to exclude staged non-IR PCI related MI in the analysis of non-IR UMI. Patients treated with multivessel PCI for not only culprit but also non-culprit territory lesions during the index emergent PCI were excluded from the final analysis. A representative case of emergent PCI with multimodality coronary imaging (preprocedural OCT, preprocedural CCTA, and postprocedural CMR) is shown in Fig. 1. The study protocol was in accordance with the Declaration of Helsinki and was approved by the Institutional Ethics Committee (TKGH-IRB 2022FY50). All patients provided written informed consent before enrollment in the institutional registry for future investigation.

Emergent coronary angiography and PCI

Invasive coronary angiography (CAG) and revascularization of the IR lesion were performed by ad hoc PCI via the routine use of drug-eluting stents using a 6-French system. All patients subsequently underwent uncomplicated PCI

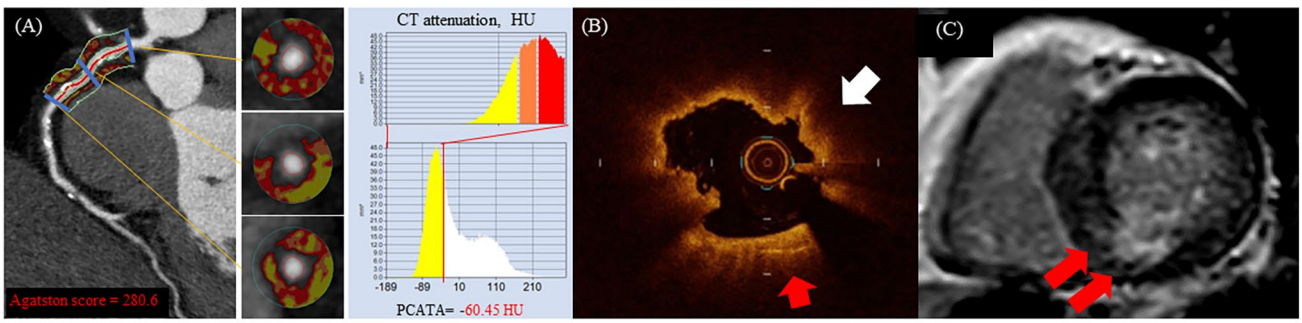

Fig. 1 Representative cardiac images of the patient with unrecognized myocardial infarction. A 61-year-old man with non-IR UMI who underwent successful PCI with multimodality coronary imaging to culprit lesion in RCA. (**A**) RCA PCATA = -60.45 HU. PCATA was defined as the mean CT attenuated value within a radial distance equal to the diameter of the vessel. Voxel histograms of CT attenuation were plotted and the mean CT attenuation of all voxels between − 190 to − 30 HU. Agatston score = 280.6. (**B**) Culprit vessel cross-sectional image of the culprit coronary artery, showing OCT-PR (white arrow), and OCT-CC (red arrow) (**C**) Short axis view of delayed-enhancement cardiac magnetic resonance imaging with inferior gadolinium enhancement (red arrow). Non-IR, non-infarct-related; UMI, unrecognized myocardial infarction; PCI, percutaneous coronary intervention; RCA, right coronary artery; PCATA, pericoronary adipose tissue attenuation, OCT, optical coherence tomography; PR, plaque rupture; CC, cholesterol crystal; CT, computed tomography

with an early invasive strategy within < 24 h after admission [14]. Coronary angiograms were analyzed quantitatively using the QAngio XA system (Medis Medical Imaging Systems, Leiden, the Netherlands). The IR lesion was identified by a combination of CCTA findings, electrocardiography (ECG), echocardiography, coronary angiography, and OCT findings by two expert interventionalists. The stent type and procedure strategy were selected at the operator's discretion.

CMR Examination: CMR acquisition and assessment of IR (ACS Culprit) scar and non-IR UMI

Images were acquired on a 1.5-T scanner (Philips Achieva, Philips Medical Systems, Best, the Netherlands) with 32-channel cardiac coils within 14 days after the IR lesion PCI and before the staged PCI of significant non-IR lesions. A detailed description of the CMR acquisition is presented in the Supplementary Materials, as previously reported [15]. LGE with a subendocardial segmental distribution was defined as UMI. The infarcted myocardium was quantified on the LGE images as myocardium with a signal intensity exceeding the mean signal intensity of the remote myocardium by >5 standard deviations (SDs) using a semi-automatic algorithm. Non-IR UMI was defined as the absence of MI/PCI/coronary artery bypass graft surgery history in medical records, and without the presence of LGE in the non-IR territories. This was confirmed by a consensus of two experienced cardiologists (K.S. and M.H.) and controlled by an expert reader (T.K.), masked to the patient data. All CMR images were analyzed using dedicated offline software (AZE Virtual Place, Canon Medical Systems Corporation, Japan).

Coronary CT-angiography acquisition and analysis

CCTA was performed exclusively using a 320-slice CT scanner (Aquilion ONE; Canon Medical Systems Corporation, Otawara, Tochigi, Japan), in accordance with the Society of Cardiovascular Computed Tomography guidelines, as previously reported [16]. Details are described in the Supplementary Material. Plaque assessment of the target lesions on CCTA was independently performed by two experienced readers (M.H. and T.M.) using the reconstructed CCTA images, transferred to an offline workstation (Ziostation2; Ziosoft Inc., Japan), as previously reported [17]. Coronary lesions were evaluated for the presence of high-risk plaque features (HRPF) [18].

Analysis of pericoronary adipose tissue and epicardial fat

Pericoronary adipose and tissue attenuation (PCATA) analyses were performed using semiautomated software (Aquarius iNtuition Edition version 4.4.13; TeraRecon Inc., Foster City, CA, USA) as previously described [19]. Pericoronary adipose tissue was defined as all voxels with attenuation between − 190 HU and − 30 HU within a radial distance from the outer vessel wall equal to the diameter of the coronary vessel. PCATA analysis was performed as the average CT attenuation of adipose tissue within the defined region of interest. PCATA was measured in the proximal 40-mm segment of the left anterior descending (LAD) coronary artery and left circumflex (LCx) coronary artery in the proximal 10- to 50-mm segment of the right coronary artery [20]. To evaluate the importance of inflammation in the culprit vessel for the presence of non-IR UMI, both PCATA in culprit vessels and PCATA in non-culprit vessels were measured, regardless of whether the vessel had UMI or not. We also calculated the mean PCATA score of the three major coronary arteries in each patient.

Epicardial fat volume (EFV) and attenuation (EFA) were quantified offline on non-contrast CT images in all patients using semiautomatic software equipped with a dedicated workstation (AZE Virtual Place, Canon Medical Systems Corporation, Japan). The region of interest (ROI) was drawn by manual tracing of the pericardium in axial planes from the takeoff of the right pulmonary artery to the apex of the heart. Then, epicardial fat volume and attenuation were automatically calculated from the sum of all pixels within a window of -190 and − 30 HU in the ROI.

Optical coherence tomography image acquisition and analysis

CT imaging was performed prior to PCI for the culprit lesion. OCT imaging was performed as previously described [21, 22]. OCT examinations were performed using Abbott's OCT (Ilumien Optis, Abbott Vascular, Santa Clara, CA, USA) or Terumo's optical frequency-domain imaging system (Lunawave, Terumo Corporation, Tokyo, Japan). OCT pullback was performed automatically by a dedicated device during the injection of flushing agents, either contrast medium or low-molecular-weight dextran with Ringer's lactate solution, at a flow rate of 3–4 mL/s via the guiding catheter using an automated power injector pump. All OCT images were analyzed using an offline review workstation by two independent investigators who were blinded to the clinical and CMR data. Briefly, a 30-mm segment of the culprit lesion (15-mm proximal and 15-mm

distal to the most stenotic lesion site) was examined in all culprit vessels.

Cross-sectional OCT images were analyzed at 1-mm intervals. The minimal lumen area (MLA) was defined as the smallest lumen area within the plaque length. Plaque rupture (PR) was identified by the presence of fibrous cap discontinuity with communication between the lumen and inner core of the plaque or with cavity formation within the plaque. Plaque erosion (PE) was defined as the presence of an attached thrombus overlying an intact plaque or luminal surface irregularity at the culprit lesion. A thrombus was defined as an irregular mass with a minimal diameter of >250 μm, adherent to the vessel wall or floating within the lumen (15). Culprit lesions were divided into the following three categories according to OCT findings: lesions characterized by PR, lesions characterized by PE, and lesions with massive thrombi precluding the assessment of plaque morphology over 90° of circumferences. Lesions in the MT group were excluded from the final analysis because of the difficulty in identifying a plaque as PR or PE. Lipids were defined as signal-poor regions with poorly defined or diffuse borders, and the degree of lipid arc was measured in lipid plaques. The fibrous cap thickness (FCT) overlying a lipid plaque was measured three times at its thinnest part, and the average value was calculated. Lipid-rich plaques were defined as those with a maximal lipid arc of $>90°$. Thin-cap fibroatheroma (TCFA) was defined as a plaque with a maximal lipid arc of $>90°$ and its thinnest FCT ≤ 80 μm [23]. Macrophage accumulation was defined as the presence of highly scattered focal regions within a fibrous cap. Microvessels were defined as signal-poor structures with vesicular or tubular shapes. Cholesterol crystals were identified as thin, linear regions of high signal intensity with high backscattering within a plaque. Calcification was defined as signal-poor or heterogeneous regions with sharply delineated borders, and the degree of the calcification arc was measured in calcified plaques. Layered plaques were identified by the presence of one or more signal-rich layers of different optical densities and a clear demarcation from the underlying plaque components [24].

Statistical analysis

Statistical analysis was performed using SPSS version 25.0 (SPSS, Inc., Chicago, IL, USA) and R version 4.0.3 (The R Foundation for Statistical Computing, Vienna, Austria) software. Categorical data were expressed as absolute frequencies and percentages and were compared using χ^2 or Fisher's exact tests. Continuous variables were expressed as mean ± standard deviation for normally distributed variables or as median (25th–75th percentile) for non-normally distributed variables and were compared using Student's *t*-tests and the Mann-Whitney U-test, respectively. The patients were divided into two groups: those with and without non-IR UMI. Clinical, pre-PCI angiographic, OCT, CCTA, and post-PCI DE-CMR data were compared between the two groups. A univariate logistic regression model was used to identify the independent predictors of UMI. Receiver operating curves (ROC) were analyzed to assess the best cut-off values of PCATA in the culprit vessel and the Agatston score for predicting the presence of non-IR UMI. The optimal cutoff value was calculated using the Youden index. A two-sided $p<0.05$ was considered statistically significant.

Results

Baseline patient characteristics and angiographical findings

Between January 2013 and May 2020, 99 patients who presented with NSTE-ACS underwent complete clinical, pre-PCI angiographic, OCT, CCTA, and post-PCI DE-CMR assessments and were initially identified and enrolled in this study. From these patients, 9 patients were excluded because of unidentified culprit lesions. Of the remaining patients, 21 patients were further excluded from the final analysis for the following reasons: 8 patients with underlying mechanisms other than plaque rupture or plaque erosion (6 patients, massive thrombus; 2 patients, calcified nodule); 2 patients with culprit lesions located in the left main artery, and 11 patients with poor imaging quality. Thus, a total of 69 patients were included in the final analysis.

In the total cohort, non-IR UMI was detected in 11 patients (15.9%). The baseline characteristics of the patients, divided according to the presence or absence of UMI, are presented in Table 1. The median age of the 69 patients was 63.0 (59–72) years, and 84.1% were men. Compared with patients without UMI, those with UMI had a lower ejection fraction (EF). The location of the culprit vessel was not significantly different between the two groups ($p=0.096$).

Multimodality coronary imaging findings for the presence of non-IR UMI

CCTA and CMR findings are presented in Table 2. The Agatston score and prevalence of high PCATA values in the culprit vessels (≥-71.3) were significantly higher in patients with non-IR UMI. LV mass volume, EFV, and EFA were not significantly associated with the presence of non-IR UMI. No significant difference in the prevalence of HRPF was detected between patients with UMI, compared with those without UMI. ROC analysis revealed that the optimal cut-off values of the Agatston score and PCATA value in

Table 1 Baseline characteristics

	Total	Patients with non-IR UMI	Patients without non-IR UMI	P value
	(n = 69)	(n = 11)	(n = 58)	
Age, (years)	63 (59–72)	69 (62–77)	63 (58–69)	0.131
Male, n (%)	58 (84.1%)	10 (90.9%)	48 (82.8%)	0.679
Hypertension, n (%)	46 (66.7%)	6 (54.5%)	40 (69.0%)	0.487
Diabetes mellitus, n (%)	21 (30.4%)	11 (36.7%)	39 (30.5%)	0.519
Hyperlipidemia, n (%)	37 (53.6%)	4 (36.4%)	33 (56.9%)	0.356
Smoker, n (%)	34 (49.3%)	5 (45.5%)	29 (50.0%)	1.000
LDL-cholesterol (mg/dl)	120 (108–151)	111 (97–139)	122 (109–152)	0.215
eGFR (ml/min/1.73m2)	73.8 (65.2–83.6)	69.6 (62.4–76.4)	75.5 (65.9–84.6)	0.309
Ejection fraction (%)	62.0 (55–66)	55.0 (51–60)	63.0 (58–66)	< 0.001
Troponin I (ng/l)	130.0 (38.0-465.0)	86.0 (56.5-271.5)	133.5 (32.0-482.3)	0.896
CRP (mg/dl)	0.09 (0.03–0.33)	0.20 (0.08–0.36)	0.09 (0.03–0.32)	0.435
GRACE score	112 (102–142)	142 (108–154)	112 (102–132)	0.173
Quantitative Coronary Angiography				
Diameter stenosis (%)	87.0 (79.6–92.4)	87.2 (77.8–88.5)	87.0 (81.1–92.4)	0.539
Reference diameter (mm)	2.84 (2.39–3.22)	2.77 (2.52–3.08)	2.88 (2.36–3.25)	0.787
Minimum lumen diameter (mm)	0.34 (0.22–0.56)	0.41 (0.31–0.56)	0.33 (0.21–0.60)	0.398
Culprit lesion location (RCA/LAD/LCx)	15/38/16	0/9/2	15/29/14	0.096
Gensini score	20 (12–32)	20 (18–68)	20 (12–32)	0.297

Non-IR, non-infarct-related; UMI, unrecognized myocardial infarction; LDL, low density lipoprotein cholesterol, eGFR, estimated glomerular filtration rate, CRP, C-reactive protein, GRACE, Global registries of acute coronary events, RCA, right coronary artery, LAD, left anterior descending artery, LCx, left circumflex coronary artery

Table 2 CCTA and CMR findings

	Total	Patients with non-IR UMI	Patients without non-IR UMI	P value
	(n = 69)	(n = 11)	(n = 58)	
High risk plaque features				
Low attenuation plaque, n (%)	43 (62.3%)	7 (63.6%)	36 (62.1%)	1.000
Napkin ring sign, n (%)	13 (18.8%)	4 (36.4%)	9 (15.5%)	0.199
Spotty calcification, n (%)	36 (52.2%)	8 (72.7%)	28 (48.3%)	0.192
Positive remodeling ≧ 1.10, n (%)	41 (59.4%)	7 (63.6%)	34 (58.6%)	1.000
Agatston sore	162.8 (45.1–538.0)	424.1 (295.3–982.0)	111.3 (18.2-422.7)	0.007
Left ventricular mass (mm^3)	94.6 (92.4–97.9)	94.4 (92.7–96.8)	94.8 (92.5–98.1)	0.439
Epicardial fat				
Epicardial fat attenuation (HU)	-78.2 (-81.6 to -74.0)	-78.3 (-82.6 to -75.1)	-78.1 (-80.7 to -73.8)	0.528
Epicardial fat volume (cm3)	29.7 (28.5–32.1)	29.4 (28.8–30.5)	29.8 (28.4–32.4)	0.682
Pericoronary fat				
PCATA in culprit vessel (HU)	-69.4 (-74.3 to -64.8)	-65.6 (-69.7 to -63.6)	-70.5 (-74.9 to -65.3)	0.121
PCATA in culprit vessel ≥-71.3	39 (56.5%)	10 (90.0)	29 (50.0)	0.018
Mean PCATA in non culprit vessel	-69.0 (-73.9 to -64.7)	-67.6 (-73.1 to -63.3)	-69.2 (-74.0 to -65.1)	0.436
Mean PCATA in three vessels	-69.0 (-74.9 to -66.0)	-67.3 (-71.3 to -62.6)	-69.3 (-75.0 to -66.1)	0.238
LGE volume by DE-CMR				
Total LGE volume (mm3)	0.7 (0.0-4.3)	4.2 (3.5–7.1)	0.0 (0.0-3.6)	0.002
Non-IR LGE volume (mm3)	0.0 (0.0–0.0)	5.4 (2.7–7.1)		

CCTA, coronary computed tomography angiography, PCATA, pericoronary adipose tissue attenuation, DE-CMR, delayed-enhancement cardiac magnetic resonance, LGE, late gadolinium-enhancement. Other abbreviations are shown in Table 1

the culprit vessel for predicting non-IR UMI were 205.22 and −71.3, respectively. PCATA in culprit vessels tended to be associated with the presence of non-IR UMI, whereas PCATA values in non-culprit vessels and the mean PCATA value in the three vessels were similar. In 11 patients with non-IR UMI, the median LGE volume was 5.4 (2.7–7.1) g. The OCT findings are shown in Table 3. Patients with non-IR UMI had higher prevalence of OCT-PR and OCT-CC than those without UMI. Compared with OCT-defined culprit lesion plaque erosion, the prevalence of high PCATA

Table 3 OCT findings

	Total	Patients with non-IR UMI	Patients without non-IR UMI	P value
	(n = 69)	(n = 11)	(n = 58)	
Plaque rupture	39 (56.5)	10 (90.0)	29 (50.0)	0.018
Plaque erosion	30 (43.5)	1 (9.1)	29 (50.0)	0.018
Lipid-rich plaque	61 (88.4)	11 (100)	50 (86.2)	0.338
Thin-cap fibroatheroma	35 (50.7)	8 (72.7)	27 (46.6)	0.188
Macrophage	60 (86.8)	10 (90.9)	50 (86.2)	1.000
Microvessel	36 (52.2)	6 (54.5)	30 (51.7)	1.000
Cholesterol crystal	23 (33.3)	7 (63.6)	16 (27.6)	0.034
Layered plaque	41 (59.4)	7 (63.6)	34 (58.6)	1.000
Thrombus	49 (71.0)	10 (90.0)	39 (67.2)	0.157
Red thrombus	24 (34.8)	6 (54.5)	18 (31.0)	0.172
Max lipid arc	267.1 (221.7-319.9)	250.0 (223.0-321.0)	272.0 (219.0-318.0)	0.779
Lipid index	1757.4 (1062.6-2482.5)	1865.0 (1175.0-2658.0)	1493.0 (1007.0-2147.0)	0.195

OCT, optical coherence tomography; non-IR, non-infarct-related; UMI, unrecognized myocardial infarction

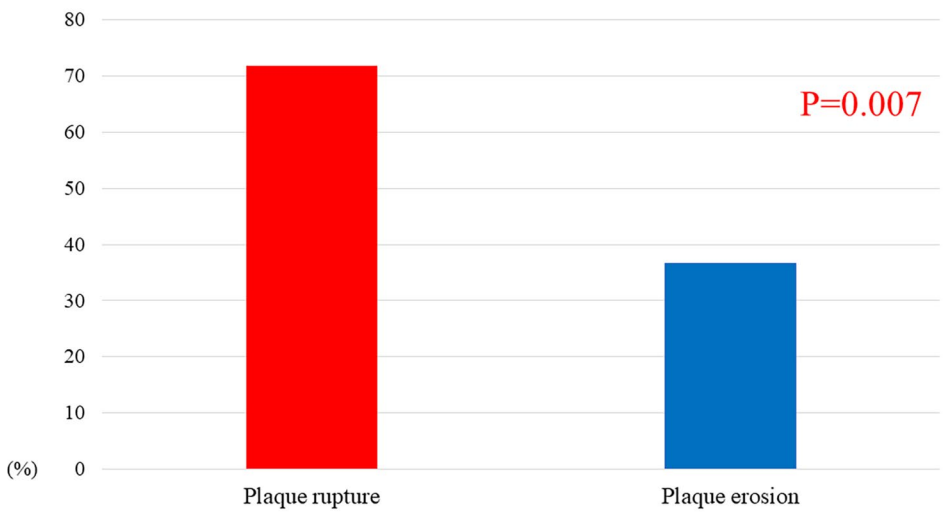

Fig. 2 Prevalence of lesions with high inflammation according to culprit plaque morphology. Compared with plaque erosion in the culprit vessel, the prevalence of vessels with high PCATA (≥-71.3) was significantly higher in the plaque rupture phenotype PCATA, pericoronary adipose tissue attenuation

in culprit vessels (≥-71.3) was higher in patients with OCT-PR (71.8% vs. 36.7%, p = 0.007) (Fig. 2).

Determinants of the presence of non-IR UMI

Lower EF, higher Gensini score, PCATA of ≥-71.3 in the culprit vessel, Agatston score of ≥ 205.22, OCT-defined culprit lesion plaque rupture (OCT-PR), and OCT-defined culprit lesion cholesterol crystal (OCT-CC) were significantly associated with the presence of non-IR UMI (Table 4).

When the total cohort was divided into four groups according to the presence of two OCT-derived risk factors (OCT-PR and OCT-CC), patients with all of the non-IR UMI risk factors showed a 37.5% (6/16) prevalence of non-IR UMI, whereas none of 23 patients without these factors showed non-IR UMI (Fig. 3). According to the presence of two OCT-derived risk factors using the cutoff values of the Agatston score (≥ 205.22) and PCATA in the culprit vessel (≥-71.3), patients with these risk factors showed a 40.9% (9/22) prevalence of non-IR UMI, whereas none of 21 patients without these risk factors showed non-IR UMI (Fig. 4).

The prevalence stratified by the number of the significant two OCT predictors (OCT-PR and OCT-CC) and two CCTA predictors (PCATA in culprit vessel of ≥-71.3 and Agatston score of ≥ 205.22) are presented in Fig. 5. When all patients were stratified by the number of these four relevant OCT and CCTA predictive features of non-IR UMI, the frequency of non-IR UMI increased according to the number of these factors (p < 0.001), compared with 2.2% (1/46) of patients with low risk factors (≤ 2).

Discussion

The present study evaluated potential predictors of the presence of non-IR UMI using urgent pre-PCI CCTA and OCT findings in patients with a first clinical episode of

Table 4 Univariate logistic regression analysis of predicting patients with non-IR UMI

	Univariate analysis		
	OR	95%CI	P value
Age	1.04	0.98–1.10	0.236
Ejection fraction	0.92	0.86–0.99	0.026
Napkin ring sign	3.11	0.75–12.90	0.117
Grace score	1.02	0.99–1.04	0.150
Gensini score	1.04	1.01–1.07	0.021
Agatston score	1.00	1.00–1.00	0.021
PCATA in culprit vessel ≥-71.3	10.0	1.2–83.2	0.033
OCT plaque rupture	10.0	1.2–83.2	0.033
OCT cholesterol crystal	4.6	1.2–17.8	0.028

Non-IR, non-infarct-related; UMI, unrecognized myocardial infarction; PCATA, pericoronary adipose tissue attenuation, OCT, optical coherence tomography; OR, odds ratio; CI, Confidence interval

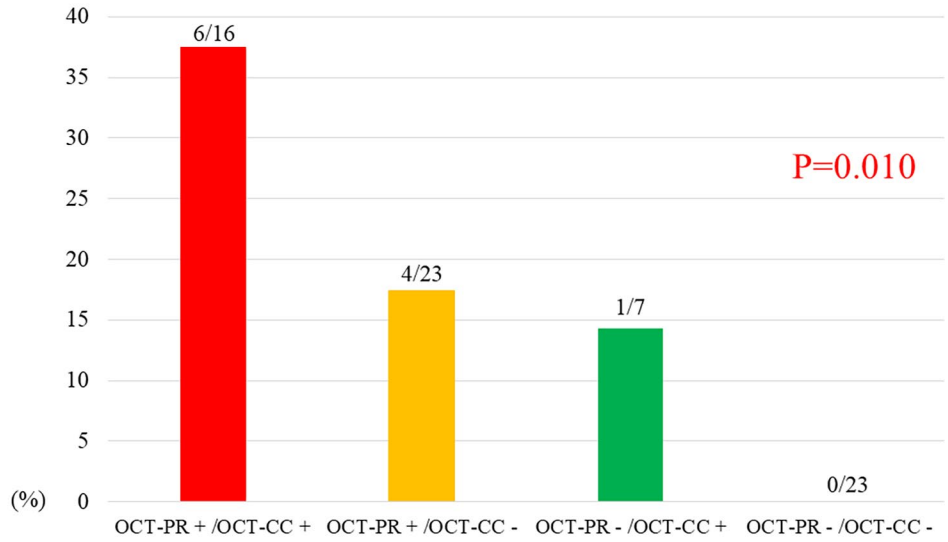

Fig. 3 Prevalence of patients with non-IR UMI according to the presence of OCT-derived risk factors. The patients were divided into four categories according to the presence of two OCT-derived risk factors (OCT-PR and OCT-CC). When culprit lesions showed all of these non-IR UMI risk factors, the prevalence of non-IR UMI was 37.5% (6/16), whereas none of 23 patients without these factors showed non-IR UMI. Non-IR, non-infarct-related; UMI, unrecognized myocardial infarction; OCT, optical coherence tomography; PR, plaque rupture; CC, cholesterol crystal

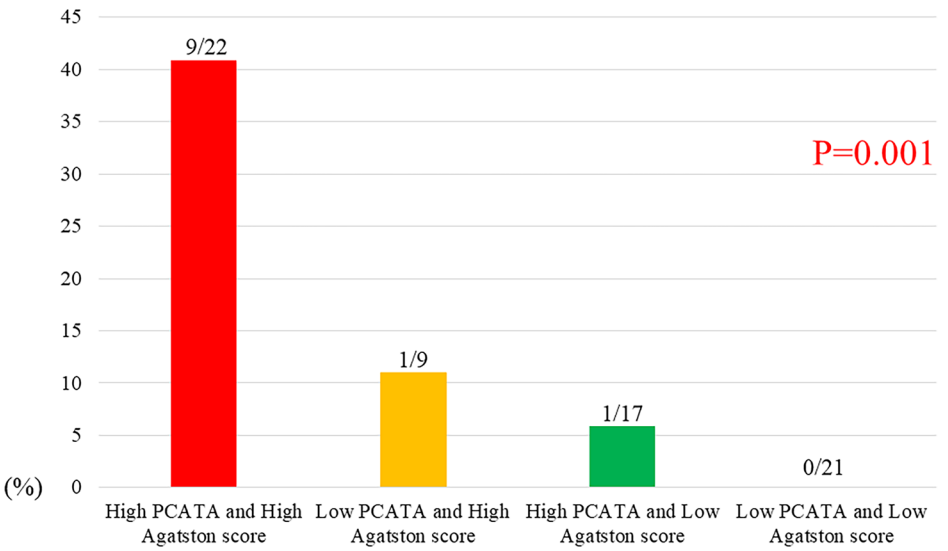

Fig. 4 Prevalence of patients with non-IR UMI according to the presence of CCTA-derived risk factors. Patients were divided into four categories according to the presence of two OCT-derived risk factors, using the cutoff values of the Agatston score (≥205.22) and PCATA in the culprit vessel (≥-71.3). When culprit lesions showed all of these risk factors, the prevalence of non-IR UMI was 40.9% (9/22), whereas none of 21 patients without these risk factors showed non-IR UMI. Non-IR, non-infarct-related; UMI, unrecognized myocardial infarction; PCATA, pericoronary adipose tissue attenuation, OCT, optical coherence tomography

NSTE-ACS. Our results demonstrated that the prevalence of non-IR UMI was 15.9%, and the median size of non-IR

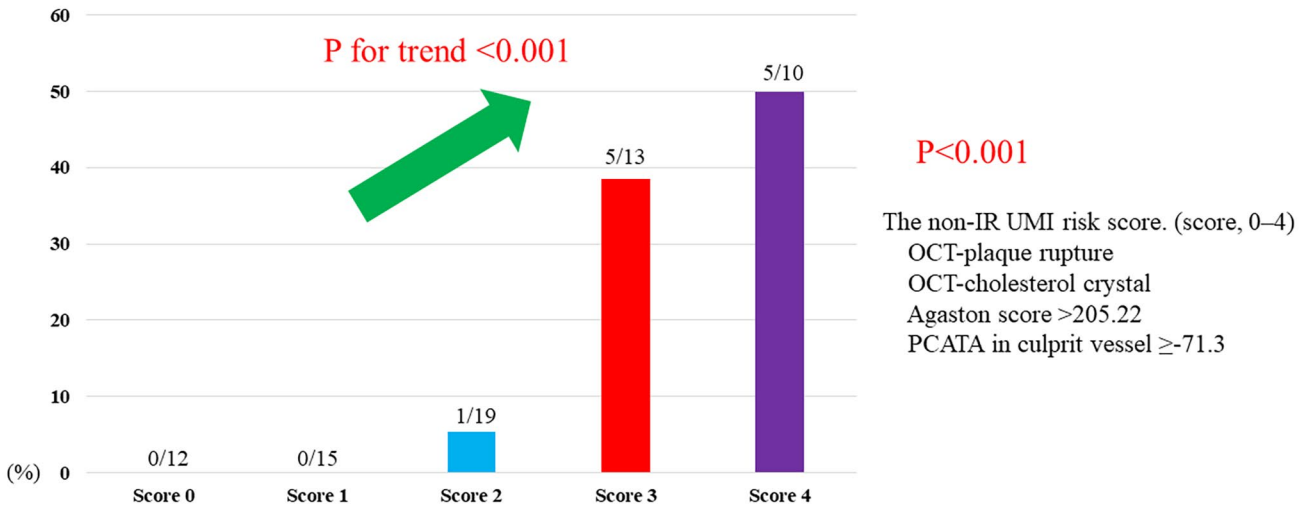

Fig. 5 Prevalence of patients with non-IR UMI according to the non-IR UMI risk score. According to the number of multimodality coronary imaging risk factors of non-IR UMI, OCT-derived risk factors (OCT-PR and OCT-CC), and CT-derived risk factors using the cutoff values of the Agatston score and PCATA in the culprit vessel, the non-IR UMI risk score was calculated (score, 0–4). As the non-IR UMI risk score increased, the prevalence of non-IR UMI also significantly increased. Non-IR, non-infarct-related; UMI, unrecognized myocardial infarction; PCATA, pericoronary adipose tissue attenuation, OCT, optical coherence tomography; PR, plaque rupture; CC, cholesterol crystal

UMI was 5.4 g. Lower EF and higher Gensini score were significantly associated with the presence of non-IR UMI. Importantly, both culprit lesion OCT-PR and OCT-CC were important predictors of the presence of non-IR UMI as well as CCTA-derived risk factors, including a high Agatston score and a high PCATA value in the culprit vessel. The frequency of non-IR UMI significantly increased according to the number of multimodality coronary imaging risk factors. When culprit lesions showed OCT-PR, OCT-CC, high Agatston score, and high PCATA in the culprit vessel, approximately half of these patients were likely to have non-IR UMI, suggesting a high risk of subsequent adverse events.

Recently, we reported that the Agatston score and mean PCATA in three vessels were independent CCTA predictors of vessels with non-IR UMI in NSTE-ACS [12]. Our results are in line with those of a previous study and extend the relationship between non-IR UMI and urgent preprocedural OCT findings. This study is the first study to demonstrate the efficacy of culprit lesion OCT findings in discriminating the presence of non-IR UMI in NSTE-ACS requiring PCI by integrating CCTA features, non-contrast CT-derived calcium score, and the CCTA-derived inflammation status of pericoronary adipose tissue.

Association between the presence of non-IR UMI and multimodality coronary imaging findings

A previous 3-vessel OCT study in patients with ACS showed that plaque rupture in culprit lesions, compared with erosion, had a higher prevalence of vulnerable plaque features (plaque rupture, macrophage accumulation, and microvessels) in non-culprit plaques [9]. Pathological studies have shown that subclinical episodes of plaque rupture are associated with pathological MI [6]. Thus, plaque rupture in culprit lesions may be a signature of silent myocardial infarction in non-IR due to high-risk plaque features, which may lead to a higher incidence of non-IR UMI. Furthermore, compared with plaque erosion, plaque rupture at the culprit site with ACS represents a higher level of pericoronary inflammation [13], as shown in Fig. 2. Non-culprit vessel high-level inflammation may be associated with the presence of UMI in the non-culprit territory. In addition, OCT enables the in vivo visualization of cholesterol crystals and is associated with features of plaque vulnerability and pericoronary inflammation [25]. A recent study showed a potential association between OCT-CC and non-culprit plaque vulnerability in ACS [26]. Since culprit vulnerable plaques in patients with ACS are associated with systemic advanced atherosclerosis, these high-risk plaques may lead to asymptomatic plaque rupture, which could result in UMI [27].

The Agatston score–derived CAC quantification provides independent and incremental information in addition to traditional risk factors for the prediction of cardiovascular events [28]. Since the Agatston score could be a signature of advanced atherosclerotic burden and pericoronary inflammation [12], the presence of non-IR UMI might represent the inter-relationship of the high-risk patient characteristics [29] associated with these features. However, no significant

association was observed between the presence of OCT-PR and Agatston score (p = 0.40). Therefore, measuring the Agatston score could provide independent and additional information over OCT assessments to identify the presence of non-IR UMI.

Notably, even when patients showed high PCATA and/or high Agatston scores, the prevalence of non-IR UMI, without high-risk culprit lesion OCT findings including OCT-PR and OCT-CC, was extremely low, suggesting that both increased pericoronary inflammation and calcium score when combined with high-risk OCT plaque features could indicate the occurrence of UMI (Fig. 5). These findings, including measurement of PCATA and Agatston score integrated with culprit lesion OCT-based plaque analysis, may enhance the identification of non-culprit UMI. The high-risk plaques linked with the progression of atherosclerosis, represented by CAC and inflammation, may lead to asymptomatic and systemic plaque ruptures and thrombosis, which could result in UMI.

Potential clinical implications

The presence of an unrecognized myocardial scar detected by LGE in patients presenting with the first NSTE-ACS has been reported to be associated with worse outcomes [1–3]. Our results demonstrated that preprocedural OCT-based plaque analysis provides additional information over CTA assessments to predict the presence of DE-CMR defined non-IR UMI, using OCT-PR, OCT-CC, Agatston score, and PCATA in the culprit vessel. Given that patients with UMI detected by DE-CMR are not likely to be identified by routine clinical work-up, our results highlight the clinical utility of CCTA and OCT in patients with NSTE-ACS. Although the current study lacks prognostic information, our findings implied that the detection of those vulnerable features on preprocedural OCT and CCTA may help identify high-risk patients accompanied by the presence of UMI, which may lead to worse cardiac outcomes. Further studies are warranted to test whether early preventive intervention following detection of UMI by DE-CMR and/or CCTA- and OCT-derived information could reduce the subsequent occurrence of UMI and adverse outcomes.

Limitations

First, this was a retrospective observational study from a single center and therefore has an intrinsic risk of selection bias. Second, a ruptured plaque phenotype may be difficult to differentiate from other plaque components such as lipids, calcifications, macrophage accumulation, or residual thrombus. Although extreme caution was exercised when reading the underlying structure by the two expert reviewers in this study, massive thrombi or calcified plaques were excluded from the final analysis because of the difficulty in judging the plaque phenotype. Third, long-term clinical outcomes were not evaluated. Fourth, patients were enrolled with contraindications to CMR, leading to further selection bias because there were no patients with metallic device implants, bronchospasm, claustrophobia, or atrioventricular block.

Conclusions

Comprehensive culprit lesion OCT assessments, including PR and CC, as well as CCTA-derived risk factors, including high Agatston score and high PCATA in the culprit vessel, may help identify non-IR UMI in patients with a first clinical episode of NSTE-ACS. Integrated CCTA and OCT assessment may help identify the presence of non-IR UMI, potentially providing prognostic information in patients with first NSTE-ACS episode.

Supplementary Information The online version contains supplementary material available at https://doi.org/10.1007/s10554-023-02903-0.

Acknowledgements None.

Authors' contributions M.Hoshino, T.S., Y.K., M.Hada, T.N., K.N., Y.T., H.U., K.S., K.M., T.Y., and T.Sasano. analyzed and interpreted the patients' data. M.Hoshino, T.S., T.M., M.Hada, T.N., K.N., Y.T., H.U. K.S., and K.M. made effort to enroll the patients. M.Hoshino and T.K. were major contributors in writing the manuscript. All authors read and approved the final manuscript.

Funding None.

Declarations

Competing interests The authors declare no competing interests.

5 References

1. Antiochos P, Ge Y, Steel K, Bingham S, Abdullah S, Mikolich JR et al (2020) Imaging of clinically unrecognized myocardial fibrosis in patients with suspected coronary artery disease. J Am Coll Cardiol 76:945–957. https://doi.org/10.1016/j.jacc.2020.06.063
2. Acharya T, Aspelund T, Jonasson TF, Schelbert EB, Cao JJ, Sathya B et al (2018) Association of unrecognized myocardial infarction with long-term outcomes in community-dwelling older adults: the ICELAND MI study. JAMA Cardiol 3:1101–1106. https://doi.org/10.1001/jamacardio.2018.3285
3. Ishihara M, Nakao K, Ozaki Y, Kimura K, Ako J, Noguchi T et al (2017) Long-term outcomes of Non-ST-Elevation myocardial infarction without creatine kinase Elevation - The J-MINUET study. Circ J 81:958–965. https://doi.org/10.1253/circj.CJ-17-0033

4. Ingkanisorn WP, Rhoads KL, Aletras AH, Kellman P, Arai AE (2004) Gadolinium delayed enhancement cardiovascular magnetic resonance correlates with clinical measures of myocardial infarction. J Am Coll Cardiol 43:2253–2259. https://doi.org/10.1016/j.jacc.2004.02.046
5. Omori T, Kurita T, Dohi K, Takasaki A, Nakata T, Nakamori S et al (2018) Prognostic impact of unrecognized myocardial scar in the non-culprit territories by cardiac magnetic resonance imaging in patients with acute myocardial infarction. Eur Heart J Cardiovasc Imaging 19:108–116. https://doi.org/10.1093/ehjci/jex194
6. Burke AP, Kolodgie FD, Farb A, Weber DK, Malcom GT, Smialek J et al (2001) Healed plaque ruptures and sudden coronary death: evidence that subclinical rupture has a role in plaque progression. Circulation 103:934–940. https://doi.org/10.1161/01.cir.103.7.934
7. Cao M, Zhao L, Ren X, Wu T, Yang G, Du Z et al (2021) Pancoronary plaque characteristics in STEMI caused by culprit plaque erosion versus rupture: 3-Vessel OCT study. JACC Cardiovasc Imaging 14:1235–1245. https://doi.org/10.1016/j.jcmg.2020.07.047
8. Rioufol G, Finet G, Ginon I, André-Fouët X, Rossi R, Vialle E et al (2002) Multiple atherosclerotic plaque rupture in acute coronary syndrome: a three-vessel intravascular ultrasound study. Circulation 106:804–808. https://doi.org/10.1161/01.cir.0000025609.13806.31
9. Sugiyama T, Yamamoto E, Bryniarski K, Xing L, Lee H, Isobe M et al (2018) Nonculprit plaque characteristics in patients with acute coronary syndrome caused by plaque erosion vs plaque rupture: a 3-vessel optical coherence tomography study. JAMA Cardiol 3:207–214. https://doi.org/10.1001/jamacardio.2017.5234
10. Linde JJ, Kelbæk H, Hansen TF, Sigvardsen PE, Torp-Pedersen C, Bech J et al (2020) Coronary CT angiography in patients with non-ST-Segment elevation acute coronary syndrome. J Am Coll Cardiol 75:453–463. https://doi.org/10.1016/j.jacc.2019.12.012
11. Kofoed KF, Kelbæk H, Hansen PR, Torp-Pedersen C, Høfsten D, Kløvgaard L et al (2018) Early versus standard care invasive examination and treatment of patients with non-ST-segment elevation acute coronary syndrome. Circulation 138:2741–2750. https://doi.org/10.1161/CIRCULATIONAHA.118.037152
12. Matsuda K, Hoshino M, Kanaji Y, Sugiyama T, Misawa T, Hada M et al (2021) Coronary computed tomography angiographic predictors of non-culprit territory unrecognized myocardial infarction assessed by cardiac magnetic resonance in non-ST-elevation acute coronary syndrome. Front Cardiovasc Med 8:825523. https://doi.org/10.3389/fcvm.2021.825523
13. Nakajima A, Sugiyama T, Araki M, Seegers LM, Dey D, McNulty I et al (2022) Plaque rupture, compared with plaque erosion, is associated with a higher level of pancoronary inflammation. JACC Cardiovasc Imaging 15:828–839. https://doi.org/10.1016/j.jcmg.2021.10.014
14. Puymirat E, Taldir G, Aissaoui N, Lemesle G, Lorgis L, Cuisset T et al (2012) Use of invasive strategy in non-ST-segment elevation myocardial infarction is a major determinant of improved long-term survival: FAST-MI (French Registry of Acute Coronary Syndrome). JACC Cardiovasc Interv 5:893–902. https://doi.org/10.1016/j.jcin.2012.05.008
15. Kanaji Y, Yonetsu T, Hamaya R, Murai T, Usui E, Hoshino M et al (2019) Prognostic value of phase-contrast cine-magnetic resonance imaging-derived global coronary flow reserve in patients with non-ST-segment elevation acute coronary syndrome treated with urgent percutaneous coronary intervention. Circ J 83:1220–1228. https://doi.org/10.1253/circj.CJ-18-1196
16. Abbara S, Blanke P, Maroules CD, Cheezum M, Choi AD, Han BK et al (2016) SCCT guidelines for the performance and acquisition of coronary computed tomographic angiography: a report of the society of cardiovascular computed tomography Guidelines Committee: endorsed by the North American Society for Cardiovascular Imaging (NASCI). J Cardiovasc Comput Tomogr 10:435–449. https://doi.org/10.1016/j.jcct.2016.10.002
17. Hoshino M, Yang S, Sugiyama T, Zhang J, Kanaji Y, Hamaya R et al (2021) Characteristic findings of microvascular dysfunction on coronary computed tomography angiography in patients with intermediate coronary stenosis. Eur Radiol 31:9198–9210. https://doi.org/10.1007/s00330-021-07909-7
18. Puchner SB, Liu T, Mayrhofer T, Truong QA, Lee H, Fleg JL et al (2014) High-risk plaque detected on coronary CT angiography predicts acute coronary syndromes independent of significant stenosis in acute chest pain: results from the ROMICAT-II trial. J Am Coll Cardiol 64:684–692. https://doi.org/10.1016/j.jacc.2014.05.039
19. Goeller M, Achenbach S, Cadet S, Kwan AC, Commandeur F, Slomka PJ et al (2018) Pericoronary adipose tissue computed tomography attenuation and high-risk plaque characteristics in acute coronary syndrome compared with stable coronary artery disease. JAMA Cardiol 3:858–863. https://doi.org/10.1001/jamacardio.2018.1997
20. Hoshino M, Zhang J, Sugiyama T, Yang S, Kanaji Y, Hamaya R et al (2021) Prognostic value of pericoronary inflammation and unsupervised machine-learning-defined phenotypic clustering of CT angiographic findings. Int J Cardiol 333:226–232. https://doi.org/10.1016/j.ijcard.2021.03.019
21. Tearney GJ, Regar E, Akasaka T, Adriaenssens T, Barlis P, Bezerra HG et al (2012) Consensus standards for acquisition, measurement, and reporting of intravascular optical coherence tomography studies: a report from the International Working Group for Intravascular Optical Coherence Tomography standardization and validation. J Am Coll Cardiol 59:1058–1072. https://doi.org/10.1016/j.jacc.2011.09.079
22. Hoshino M, Yonetsu T, Usui E, Kanaji Y, Ohya H, Sumino Y et al (2019) Clinical significance of the presence or absence of lipid-rich plaque underneath intact fibrous cap plaque in acute coronary syndrome. J Am Heart Assoc 8:e011820. https://doi.org/10.1161/JAHA.118.011820
23. Ozaki Y, Okumura M, Ismail TF, Motoyama S, Naruse H, Hattori K et al (2011) Coronary CT angiographic characteristics of culprit lesions in acute coronary syndromes not related to plaque rupture as defined by optical coherence tomography and angioscopy. Eur Heart J 32:2814–2823. https://doi.org/10.1093/eurheartj/ehr189
24. Russo M, Fracassi F, Kurihara O, Kim HO, Thondapu V, Araki M et al (2020) Healed plaques in patients with stable angina pectoris. Arterioscler Thromb Vasc Biol 40:1587–1597. https://doi.org/10.1161/ATVBAHA.120.314298
25. Lin A, Nerlekar N, Munnur RK, Kataoka Y, Andrews J, Dey D et al (2020) Cholesterol crystal-induced coronary inflammation: insights from optical coherence tomography and pericoronary adipose tissue computed tomography attenuation. J Cardiovasc Comput Tomogr 14:277–278. https://doi.org/10.1016/j.jcct.2019.11.011
26. Qin Z, Cao M, Xi X, Zhang Y, Wang Z, Zhao S et al (2022) Cholesterol crystals in non-culprit plaques of STEMI patients: a 3-vessel OCT study. Int J Cardiol 364(364):162–168. https://doi.org/10.1016/j.ijcard.2022.06.016
27. Mann J, Davies MJ (1999) Mechanisms of progression in native coronary artery disease: role of healed plaque disruption. Heart 82:265–268. https://doi.org/10.1136/hrt.82.3.265
28. Budoff MJ, Shaw LJ, Liu ST, Weinstein SR, Mosler TP, Tseng PH et al (2007) Long-term prognosis associated with coronary calcification: observations from a registry of 25,253 patients. J Am Coll Cardiol 49:1860–1870. https://doi.org/10.1016/j.jacc.2006.10.079
29. Cha MJ, Kim SM, Kim Y, Kim HS, Cho SJ, Sung J et al (2018) Unrecognized myocardial infarction detected on cardiac magnetic

resonance imaging: association with coronary artery calcium score and cardiovascular risk prediction scores in asymptomatic asian cohort. PLoS ONE 13:e0204040. https://doi.org/10.1371/journal.pone.0204040